THE BELL SYSTEM TECHNICAL JOURNAL

DEVOTED TO THE SCIENTIFIC AND ENGINEERING ASPECTS OF ELECTRICAL COMMUNICATION

Volume 58 October 1979 Number 8

Unbiased Spectral Estimation and System Identification Using Short-Time Spectral Analysis Methods

By J. B. ALLEN and L. R. RABINER

(Manuscript received March 16, 1979)

The methods of system identification and spectral analysis are well documented in the literature. In this paper, we attempt to merge the methods of least-square system identification and short-time Fourier transform spectral estimation. Starting from the least-squares normal equations for a linear system identification problem and expanding the signals in short-time Fourier transforms, we derive a Toeplitz system of equations, the solution of which approximates the original least-squares equation solution. We then bound the error norm between the two solution methods and show the properties of the error by numerical methods. The resulting "spectral" estimation method is shown to completely remove the bias normally associated with previously proposed spectral estimation procedures. The method appears to be particularly useful when one is interested in linear system identification of very large systems (long impulses response) or for system identification in the presence of nonstationary (e.g., burst) noise. Extensive numerical results are included.

I. INTRODUCTION

Although time-domain methods have been in use for system identification and modeling for at least 35 years, no simple, robust procedure has been proposed which uses short-time Fourier transform methods. Classical spectral analysis methods are generally inadequate for all but the simplest cases because of their unsatisfactory properties.

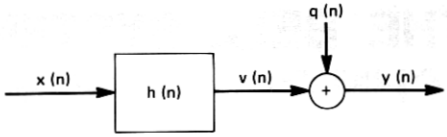

Fig. 1—Block diagram of the system identification model.

Recent results in the theory of short-time spectral analysis have suggested a framework for a new method of spectral estimation and system identification.[1-6] It is the purpose of this paper to describe the theory of this new algorithm and to compare and contrast it to three alternative procedures of system identification. In this paper we attempt to clear up many questions raised by an earlier related paper.[1]

Figure 1 is a block diagram of the general system identification model. The input signal $x(n)$ is assumed to be zero mean white noise having variance σ_x^2. The linear system $h(n)$ is assumed to be a finite impulse response (FIR) system of duration M samples,

$$h(n) = 0, \quad n < 0, n > M - 1. \tag{1}$$

At the output of the linear system, an independent white noise $q(n)$ (having zero mean and variance σ_q^2) is added to $v(n)$ to give the output signal $y(n)$. Thus

$$y(n) = x(n) * h(n) + q(n) \tag{2a}$$

$$= \sum_{m=0}^{M-1} h(m)x(n-m) + q(n). \tag{2b}$$

The signal-to-noise ratio (s/n) at the output of the system is defined as

$$\text{s/n} = 10 \log_{10}\left(\frac{\mathbf{E}(v^2(n))}{\mathbf{E}(q^2(n))}\right) = 10 \log_{10}\left(\frac{\sigma_v^2}{\sigma_q^2}\right), \tag{3}$$

where $\mathbf{E}$ is the expectation operation.

The system identification problem is one of finding an estimate $\hat{h}(n)$ of $h(n)$, given only N samples of the input $x(n)$ and the output $y(n)$. It is assumed that the duration of $\hat{h}(n)$ (call this $\hat{M}$) satisfies the relation

$$\hat{M} \geq M, \tag{4}$$

i.e., that we have knowledge of, or can accurately bound, the duration of the system impulse response. In general, we assume that $N \gg \hat{M}$. Assuming the constraint of eq. (4) is obeyed, one reasonable measure of system performance is the quantity

$$Q = 10 \log_{10} \left[\frac{\sum_{m=0}^{\hat{M}-1} [h(m) - \hat{h}(m)]^2}{\sum_{m=0}^{\hat{M}-1} h^2(m)} \right]. \tag{5}$$

The quantity Q is called the "misadjustment" or "misalignment" between $h(n)$ and $\hat{h}(n)$.

Several classes of techniques are known in the time domain for solving the system identification problem, the most important of which is the classical least-squares analysis (LSA) method. In the frequency domain, however, only very simple, suboptimal techniques have been proposed for solving the system identification problem, and these techniques have not proven to be entirely adequate for any reasonable class of problems.[5,7] In this paper, we derive a new short-time Fourier transform domain approach to the system identification problem which alleviates many of the problems encountered using previously proposed frequency domain methods. High-quality frequency domain techniques are interesting for many reasons, but several notable ones are that (*i*) very large systems may be estimated ($\hat{M} \approx 10^3$ points), (*ii*) FFT methods are numerically very efficient, (*iii*) ill-conditioned problems are naturally identified, and (*iv*) the coherence function may be computed and used adaptively to dynamically modify the analysis procedures in a data-dependent way (a form of nonlinear analysis).[11] Furthermore, with the advent of high-speed array processors, algorithmic procedures which use FFTs are frequently easily implemented.

II. LEAST-SQUARES SOLUTION

Several basic results are necessary before we describe our frequency domain method. Since our approach is based on the method of least-squares analysis (LSA), we define that procedure first.

In the LSA method, one minimizes the quantity

$$I = \sum_{n=\hat{M}-1}^{N-1} (y(n) - \hat{y}(n))^2, \tag{6}$$

where

$$y(n) = \sum_{m=0}^{M-1} h(m)x(n-m) + q(n)$$

$$= h*x + q(n) \tag{7}$$

and

$$\hat{y}(n) = \sum_{m=0}^{\hat{M}-1} \hat{h}(m)x(n-m) = \hat{h}*x. \tag{8}$$

Taking partials of I with respect to $\hat{h}(l)$, the unknowns, for $0 \leq l \leq \hat{M} - 1$ results in the set of equations

$$\sum_{n=\hat{M}-1}^{N-1} (y(n) - \hat{y}(n))x(n - l) = 0, \qquad 0 \leq l \leq \hat{M} - 1, \tag{9}$$

or in terms of x and y

$$\sum_{m=0}^{\hat{M}-1} \hat{h}(m) \sum_{n} x(n - l)x(n - m) = \sum_{n} y(n)x(n - l), \; 0 \leq l \leq \hat{M} - 1, \tag{10}$$

where in all cases $\sum_n$ implies a sum from $\hat{M} - 1$ to $N - 1$, where N is the total number of data points required by the analysis. Our limits on n have been chosen so that the first and last required points of data are $x(0)$ and $x(N - 1)$.

We now define

$$\phi(l, m) = \sum_{n} x(n - l)x(n - m) \tag{11}$$

$$r(l) = \sum_{n} y(n)x(n - l) \tag{12}$$

$$\boldsymbol{\phi} = [\phi(l, m)] \tag{13}$$

$$\mathbf{r} = [r(l)] \tag{14}$$

$$\hat{\mathbf{h}} = [\hat{h}(l)]. \tag{15}$$

Using this notation, eq. (10) becomes the matrix equation

$$\boldsymbol{\phi}\hat{\mathbf{h}} = \mathbf{r}. \tag{16}$$

Our approach will be to approximate eq. (16) by a Toeplitz matrix equation which may be solved by one of the Toeplitz inversion methods[8,9] or approximately by DFT methods. In general, the solution of eq. (11) would be the optimal approach; however, when $\hat{\mathbf{h}}$ is very large (i.e., $\hat{M} \approx 10^3$), the computation, storage, and solution of eq. (11) is totally impractical. Under these conditions, the methods of this paper might be useful.

III. OVERLAP-ADD EXPANSIONS

The key to our method is the overlap-add expansion of a signal based on the following identity:

$$\sum_{m=-\infty}^{\infty} w(mR - n) = (1/R) \sum_{p=0}^{R-1} W(e^{j(2\pi/R)p})e^{-j(2\pi/R)np}, \tag{17}$$

where $W(z)$ is the z transform of $w(n)$ and m, R, n, p are integers. Equation (17) is the discrete version of the Poisson sum formula.[2] If

we now assume that $w(n)$ is a time-limited lowpass function, such as a Hamming or Kaiser window, and R is chosen such that $e^{j2\pi/R}$ is greater than the cutoff frequency of $W(z)$, then the following approximate relation holds:

$$(R/W(e^{j0}))\sum_{m=-\infty}^{\infty} w(mR-n)=1, \tag{18}$$

with an error determined by the out-of-band energy in the window $w(n)$. For any reasonable window, the error is negligible.[2] If we define $D=W(e^{j0})/R$ and multiply eq. (18) by any signal $x(n)$, we obtain the overlap-add expansion of $x(n)$:

$$x(n)=\sum_{m=-\infty}^{\infty} x_m(n), \tag{19}$$

where

$$x_m(n)=\frac{1}{D}w(mR-n)x(n). \tag{20}$$

The Fourier transform of $x_m(n)$ is called the "short-time" Fourier transform.[3,4] Expansions of ϕ and $\mathbf{r}$ by use of overlap-add expansions of $x(n)$ and $y(n)$ are possible through straightforward application of eqs. (19) and (11) and (12):

$$\begin{aligned}\phi(l,m)&=\sum_n\sum_{k=-\infty}^{\infty} x_k(n-l)\sum_{p=-\infty}^{\infty} x_p(n-m)\\&=\sum_{p=-\infty}^{\infty}\sum_{k=-\infty}^{\infty}\phi_{pk}(l,m),\end{aligned} \tag{21}$$

where we have defined

$$\begin{aligned}\phi_{pk}(l,m)&=\sum_n x_k(n-l)x_p(n-m)\\&=\frac{1}{D^2}\sum_n x(n-l)w(kR+l-n)\\&\quad\cdot x(n-m)w(pR+m-n)\end{aligned} \tag{22}$$

and

$$\begin{aligned}r(l)&=\sum_n y(n)x(n-l)\\&=\sum_n\sum_{p=-\infty}^{\infty}\sum_{k=-\infty}^{\infty} y_p(n)x_k(n-l)\end{aligned}$$

$$= \sum_{p=-\infty}^{\infty} \sum_{k=-\infty}^{\infty} r_{pk}(l), \tag{23}$$

where

$$r_{pk}(l) = \sum_n y_p(n) x_k(n-l)$$

$$= \frac{1}{D^2} \sum_n y(n) w(pR - n) x(n-l) w(kR + l - n). \tag{24}$$

In Fig. 2 we show the relative window displacements for the term $\phi_{pk}(l, m)$ of eq. (22) assuming a window L points long. Due to the time truncation of the windows, the sum on n does not extend beyond the interval $N_A \leq n \leq N_B$, where

$$N_A = \max(kR + l, pR + m) + 1 - L$$

$$N_B = \min(kR + l, pR + m). \tag{25}$$

The situation is identical for the case of $r_{pk}(l)$ if m is set to zero in eq. (25).

When implementing the sums on p and k, it is frequently convenient to make a linear transformation of variables from k to q of the form $k = p + q$. In these variables, N_A and N_B may be written as

$$N_A(p, q) = pR - L + 1 + \max(m, qR + l) \tag{26}$$

$$N_B(p, q) = pR + \min(m, qR + l). \tag{27}$$

IV. SHORT-TIME SPECTRAL APPROACH TO SYSTEM IDENTIFICATION

In this section, we show how to split the LSA matrix equation $\phi \mathbf{h} = \mathbf{r}$ into the sum of a Toeplitz matrix and an error matrix. The Toeplitz matrix may be evaluated in the frequency domain and inverted by Toeplitz matrix inversion methods (or approximately by DFT methods). The error matrix will be shown to decrease (relative to the Toeplitz part) as $1/N$, where N is the number of data points. Thus as N increases, the error in the solution (relative to the LSA solution) will decrease at the rate of 6 dB per octave as the number of data points

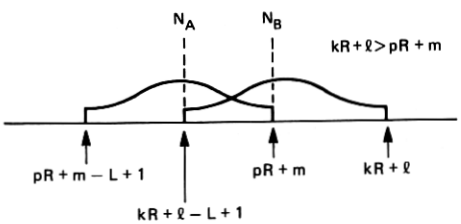

Fig. 2—Relative position of the windows for the matrix element ϕ_{pk}.

increases. Significant errors in $\bar{\mathbf{h}}$ due to the additive noise $q(n)$ are also present when the s/n is small, and these errors decrease at the rate of 3 dB per octave as N increases.[6] Thus, for large enough N, the truncation errors due to our approximation of the LSA matrix equation will be less than those due to the additive noise $q(n)$. Under these conditions, the Toeplitz estimate will be as accurate as the LSA result.

We split eq. (11) as follows

$$\begin{aligned} \boldsymbol{\phi} &= \hat{\boldsymbol{\phi}} + \boldsymbol{\epsilon} \\ \mathbf{r} &= \hat{\mathbf{r}} + \boldsymbol{\delta} \\ \bar{\mathbf{h}} &= \hat{\mathbf{h}} + \boldsymbol{\Delta}, \end{aligned} \tag{28}$$

where $\boldsymbol{\epsilon}$ is the non-Toeplitz part of $\boldsymbol{\phi}$, $\hat{\boldsymbol{\phi}}$ is Toeplitz and symmetric (i.e., $\hat{\boldsymbol{\phi}} = [\hat{\phi}(l-m)] = [\hat{\phi}(m-l)]$), and $\hat{\mathbf{h}}$ satisfies the equation

$$\hat{\boldsymbol{\phi}}\hat{\mathbf{h}} = \hat{\mathbf{r}}. \tag{29}$$

$\boldsymbol{\Delta}$ is the error between the LSA solution and the Toeplitz solution eq. (29). By bounding the norm of $\boldsymbol{\Delta}$, $\|\boldsymbol{\Delta}\| = \|\bar{\mathbf{h}} - \hat{\mathbf{h}}\|$, we can evaluate the error introduced by our procedure.

To obtain an expression for $\hat{\boldsymbol{\phi}}$, we observe the following: When N_A and N_B are inside the range of the sum on n, namely, $\hat{M} - 1 \leqslant n \leqslant N - 1$, the sum on n is limited by the windows rather than by the data. We define $\hat{\boldsymbol{\phi}}$ to be composed of all terms of $\phi_{pk}(l, m)$ of eq. (21) such that N_A and N_B lie inside the natural interval of the data independent of $l - m$ and $\boldsymbol{\epsilon}$ to include all the remaining terms of $\phi_{pk}(l, m)$. Thus

$$\hat{\phi}(l-m) = \sum_{p \in \mathbf{S}} \sum_{k \in \mathbf{S}} \phi_{pk}(l, m) \tag{30}$$

$$\hat{r}(l) = \sum_{p \in \mathbf{S}} \sum_{k \in \mathbf{S}} r_{pk}(l) \tag{31}$$

$$\epsilon(l, m) = \sum_{p \notin \mathbf{S}} \sum_{k \notin \mathbf{S}} \phi_{pk}(l, m) \tag{32}$$

$$\delta(l) = \sum_{p \notin \mathbf{S}} \sum_{k \notin \mathbf{S}} r_{pk}(l) \tag{33}$$

define the matrix elements of $\hat{\boldsymbol{\phi}}$, $\hat{\mathbf{r}}$, $\boldsymbol{\epsilon}$, and $\boldsymbol{\delta}$, respectively. For $\hat{\boldsymbol{\phi}}$ and $\hat{\mathbf{r}}$, the sums on p and k are over the set $\mathbf{S}(p, k)$, while $\boldsymbol{\epsilon}$ and $\boldsymbol{\delta}$ are summed over all k and p outside $\mathbf{S}$. The set $\mathbf{S}$ is defined by all integers p, k, as shown by the dots in Fig. 3, such that

$$\begin{aligned} N_A &\geqslant \hat{M} - 1 \\ N_B &\leqslant N - 1 \\ N_A &\leqslant N_B. \end{aligned} \tag{34}$$

Equation (34) is to be satisfied for all m and l in the range $[0, \hat{M} - 1]$. In the appendix we give an explicit formula for $\hat{\phi}(l - m)$. From Fig. 3

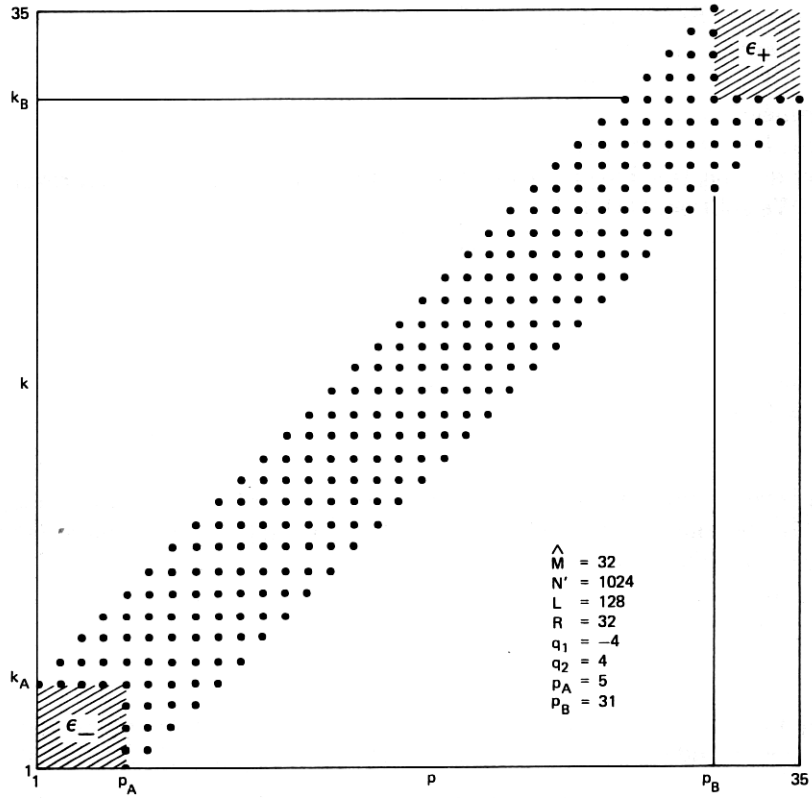

Fig. 3—Points comprising the set S in the (p, k) plane which are used in computing $\hat{\phi}$ and $\hat{r}$. Also shown are the regions which define ϵ (see the appendix).

we see that, in general, the set forms a strip which is missing small pieces at its ends. These small pieces are the set of $p, k \notin \mathbf{S}$ which may be used to compute ϵ and δ (see appendix).

Because of the definition of the set S, the sum on n in eqs. (22) and (24) may be extended to $\pm\infty$ since the windows naturally truncate the data to $N_A \leqslant n \leqslant N_B$. As a result of this definition, $\hat{\phi}$ is only a function of $l - m$ and is therefore Toeplitz. Such is not the case for $\epsilon(l, m)$, however, since most terms in this sum are truncated at either $n = \hat{M} - 1$ or $n = N - 1$. Finally, note that the expected value of elements of $\hat{\phi}$ or $\hat{\mathbf{r}}$ increases linearly in N (i.e., is of order N),

$$\mathbf{E}(\hat{\phi}) = O(N)$$

$$\mathbf{E}(\hat{r}) = O(N),$$

while the expected value of elements of ϵ and δ is of order 1 (i.e., independent of N)

$$\mathbf{E}(\delta) = O(1)$$

$$\mathbf{E}(\epsilon) = O(1).$$

Thus, as N approaches ∞, the solution of eq. (29) approaches that of eq. (16) at a rate of 6 dB per octave in N.

V. TRUNCATION ERROR ANALYSIS

A bound on the truncation errors may be obtained from eqs. (16), (28), and (29) in the following way. From eqs. (16) and (28),

$$(\hat{\phi} + \epsilon)(\hat{\mathbf{h}} + \Delta) = \hat{\mathbf{r}} + \delta \tag{35}$$

or

$$\hat{\phi}\hat{\mathbf{h}} + \hat{\phi}\Delta + \epsilon\hat{\mathbf{h}} + \epsilon\Delta = \hat{\mathbf{r}} + \delta. \tag{36}$$

As a result of eq. (29),

$$\hat{\phi}\Delta + \epsilon\hat{\mathbf{h}} + \epsilon\Delta = \delta. \tag{37}$$

Next we multiply by $\hat{\phi}^{-1}$ and solve for Δ as

$$\Delta = \hat{\phi}^{-1}(\delta - \epsilon\hat{\mathbf{h}}) - \hat{\phi}^{-1}\epsilon\Delta. \tag{38}$$

Forming the norm of each side of eq. (38), we define a measure of error Q_Δ [eq. (5)] which, after some algebra, may be shown to be bounded by ($\|\cdot\|$ as defined here is the Euclidean norm of a vector)

$$Q_\Delta = 20 \log_{10}\left[\frac{\|\Delta\|}{\|\hat{\mathbf{h}}\|}\right] \leqslant 20 \log_{10}\left[\frac{\|\hat{\phi}^{-1}\| \cdot \|\delta - \epsilon\hat{\mathbf{h}}\|}{1 - \|\hat{\phi}^{-1}\| \cdot \|\epsilon\|}\right]. \tag{39}$$

If we let $\lambda_i(\mathbf{A})$ denote the ith eigenvalue of the matrix $\mathbf{A}$, then it can be shown that

$$\|\hat{\phi}^{-1}\| = \{\min_i \lambda_i(\hat{\phi}^t\hat{\phi})\}^{-1/2}$$

$$\|\epsilon\| = \{\max_i \lambda_i(\epsilon^t\epsilon)\}^{1/2}$$

where, by definition,

$$\|\hat{\mathbf{h}}\| = \left(\sum_{l=0}^{\hat{M}-1} \hat{h}^2(l)\right)^{1/2}$$

$$\|\Delta\| = \left(\sum_{l=0}^{\hat{M}-1} \Delta^2(l)\right)^{1/2}. \tag{40}$$

Useful bounds on these norms are easily obtained for ϵ and $\hat{\phi}^{-1}$. For the latter, if $\hat{\Phi}(\omega_k)$ is the $2\hat{M} - 1$ point DFT of $[\hat{\phi}_0, \hat{\phi}_1, \cdots, \hat{\phi}_{\hat{M}-1}, \hat{\phi}_{1-\hat{M}}, \cdots, \hat{\phi}_{-1}]$, then

$$\|\hat{\phi}^{-1}\| \leq \min_{\omega_k} |\hat{\Phi}(\omega_k)|^{-1}. \tag{41}$$

In practice, $\hat{\Phi}(\omega_k)$ and the DFT of $\hat{r}$, $\hat{R}(\omega_k)$ are directly computed from the data $x(n)$ and $y(n)$. Q_Δ is only of theoretical interest and would generally not be computed in a real problem.

VI. IMPLEMENTATION OF THE SHORT-TIME SPECTRAL APPROACH TO SYSTEM IDENTIFICATION

As a result of the previous discussion, our method is implemented as follows:

(*i*) Form windowed data segments $y_p(n)$ and $x_k(n)$ for each p and k in **S**.

(*ii*) Compute the correlations $\hat{\phi}_{pk}(l-m)$ and $\hat{r}_{pk}(l)$ which may be done as follows (using fast correlation techniques):

$$\begin{aligned} X_k(\omega) &= \mathbf{F}\{x_k(n)\} \\ Y_p(\omega) &= \mathbf{F}\{y_p(n)\} \\ \hat{\Phi}_{pk}(\omega) &= X_k^*(\omega) X_p(\omega) \\ \hat{R}_{pk}(\omega) &= X_k^*(\omega)\, Y_p(\omega) \\ \hat{\phi}_{pk}(n) &= \mathbf{F}^{-1}[\hat{\Phi}_{pk}(\omega)] \\ \hat{r}_{pk}(n) &= \mathbf{F}^{-1}[\hat{R}_{pk}(\omega)]. \end{aligned} \tag{42}$$

$\mathbf{F}[\cdot]$ and $\mathbf{F}^{-1}[\cdot]$ are the Fourier transform operations and $()^*$ defines conjugation.

(*iii*) Form $\hat{\phi}(l)$ and $\hat{r}(l)$ by summing over all $p, k \in \mathbf{S}$ as discussed in the appendix. (In practice, this computation is done recursively. Furthermore, the sum is best done in the frequency domain.)

(*iv*) (Solution Method 1) Finally, solve the matrix equation

$$\hat{\boldsymbol{\phi}}\hat{\mathbf{h}} = \hat{\mathbf{r}}.$$

This equation may be solved by Toeplitz matrix inversion methods which require only $\hat{M}^2$ operations and $2\hat{M}$ storage locations.

(*iv'*) (Solution Method 2) Alternatively, under some conditions we may approximately find $\hat{H}(\omega)$ by Fourier transforms from

$$\hat{\Phi}(\omega) = \mathbf{F}\left[\sum_{p\in\mathbf{S}}\sum_{k\in\mathbf{S}} \hat{\phi}_{pk}(l)\right]$$

$$\hat{R}(\omega) = \mathbf{F}\left[\sum_{p\in\mathbf{S}}\sum_{k\in\mathbf{S}} \hat{r}_{pk}(l)\right]$$

$$\hat{H}(\omega) = \frac{\hat{R}(\omega)}{\hat{\Phi}(\omega)}.$$

$\hat{\Phi}(\omega)$ is the autospectral estimate and $\hat{R}(\omega)$ is the cross-spectral estimate. They sharply differ from the classical definitions of these quantities because the cross terms $p \neq k$ have been included. The inclusion of these cross terms is responsible for the removal of the bias in these estimates (see the next section). The DFT version of the above differs slightly in some of its details.

VII. BIAS AND THE CLASSICAL CASE OF SPECTRAL ESTIMATION

The most common method of spectral estimation is equivalent to forming the estimate

$$S_{xy}(\omega) = \sum_k Y_k(\omega) X_k^*(\omega), \tag{43}$$

where the sum on k is taken on nonoverlapping or slightly overlapping intervals (i.e., $R = L$ or $R = L/2$). There appear to be several flaws in this method. First, R should be less than L/Ω where Ω is the time-bandwidth product of the window, as is required by the Nyquist theorem.[2-4] For a Hamming window, Ω is 4. Second, because of the absence of cross terms, bias is present in the estimate as may be seen by inverse Fourier transforming $S_{xy}(\omega)$. For example, if in eqs. (29) to (31) we modify the sum on k to be $k = p + q$ with q a fixed integer, then eq. (29) becomes

$$\sum_{m=0}^{\hat{M}-1} \hat{h}(m) \sum_p \hat{\phi}_{p,p+q}(l-m) = \sum_p \hat{r}_{p,p+q}(l). \tag{44}$$

If we define the (decimated) autocorrelation of the window by

$$\psi_w(l) = \sum_p w(pR) w(pR + l), \tag{45}$$

then, for a white noise input (with variance σ_x^2) and for no additive noise ($\sigma_q^2 = 0$), if we assume ergodicity, i.e.,

$$\lim_{N\to\infty}\left[\frac{1}{N}\sum_{n=0}^{N-1} x(n)x(n+m)\right] = \sigma_x^2\delta(m) = \mathbf{E}[x(n)x(n+m)], \tag{46}$$

where $\delta(m)$ is one when $m = 0$ and zero otherwise, the term in the left-hand side of eq. (44) reduces to (as $N \to \infty$)

$$\lim_{N\to\infty}\left[\frac{1}{N}\sum_p \hat{\phi}_{p,p+q}(l-m)\right] = \lim_{N\to\infty}\left[\frac{1}{N}\sum_{n=0}^{N-1} x(n-m)x(n-l) \sum_p w(pR+m-n) \cdot w((p+q)R+1-n)\right] \tag{47}$$

$$= \sigma_x^2\delta(m-l)\psi_w(qR+l-m) \tag{48}$$

and the right-hand side of eq. (44) similarly reduces to

$$\lim_{N\to\infty}\left[\frac{1}{N}\sum_{p}\hat{r}_{p,p+q}(l)\right] = \lim_{N\to\infty}\left[\frac{1}{N}\sum_{n=0}^{N-1} y(n)x(n-l) \sum_{p} w(pR-n)w((p+q)R+l-n)\right] \quad (49)$$

$$= \sigma_x^2 h(l)\psi_w(qR+l). \quad (50)$$

From eqs. (44), (48), and (50), we get

$$\sigma_x^2 \hat{h}(l)\psi_w(qR) = \sigma_x^2 h(l)\psi_w(qR+l) \quad (51)$$

or

$$\hat{h}(l) = h(l)\frac{\psi_w(qR+l)}{\psi_w(qR)}. \quad (52)$$

Equation (52) shows that the effect of the window is to modify the estimate of h by the quantity $\psi_w(qR+l)/\psi_w(qR)$. When $q=0$ [the classical case, eq. (43)], we have the result

$$\hat{h}(l) = h(l)\frac{\psi_w(l)}{\psi_w(0)}; \quad (53)$$

thus, $\hat{h}(l)$ is a biased version of $h(l)$. By summing over q [i.e., sum eq. (44) over q], the bias is removed since ψ_w is a lowpass function, satisfying the relation [see eq. (18)]

$$\sum_{q}\psi_w(qR+l) = \sum_{q}\psi_w(qR) = \text{constant} \quad (54)$$

and eq. (52) gives the desired result

$$\hat{h}(l) = h(l), \quad (55)$$

independent of the window.

VIII. EXPERIMENTAL RESULTS

In this section, we give some numerical results for a simulated system identification problem. Using the system of Fig. 1 as the model, a specific FIR system was chosen for $h(n)$ with impulse response duration $M=7$ samples. This is the simple system used in Refs. 1 and 6, and its impulse response is given by

n	0	1	2	3	4	5	6
$h(n)$	0.1	0.5	1.0	0.5	−0.5	−1.0	0.5

The input to the system $x(n)$ was a Gaussian noise with zero mean and variance σ_x^2. The additive noise $q(n)$ was an independent Gaussian

noise with zero mean and variance σ_q^2. In each of these examples, a Hamming window was used.

Figure 4 shows a plot of Q [eq. (5)] as a function of N for $\sigma_q^2 = 0$ (i.e., no additive noise) and for values of the parameter q_0, where q_0 is the number of off-diagonal cross terms used in estimating $\hat{\boldsymbol{\phi}}$ and $\hat{\mathbf{r}}$, as expressed in the form

$$\hat{\phi}(l) = \sum_{q=-q_0}^{q_0} \sum_{p=p_1}^{p_2} \hat{\phi}_{p,p+q}(l) \tag{56}$$

$$\hat{r}(l) = \sum_{q=-q_0}^{q_0} \sum_{p=p_1}^{p_2} \hat{r}_{p,p+q}(l). \tag{57}$$

For this example, solution method 1 [Section VI, step (*iv*)] was used to solve the matrix equation. As q_0 gets larger (i.e., as more cross terms are included), the bias is removed as seen in Fig. 4. If $q_0 \geq q_{\max}$, where [see eq. (70) in the appendix]

$$q_{\max} = \left\lfloor \frac{M + L - 2}{R} \right\rfloor, \tag{58}$$

then no further changes occur in $\hat{\phi}(l)$, $\hat{r}(l)$ (or Q). In this example, $q_{\max} = 5$. The effects of the bias for $q_0 = 0$, 1, 2, and 3 are such that, for large values of N, Q is from 15 to 45 dB worse than for the unbiased estimates. For values of q_0 greater than 3, only small changes occur in Q. Thus there is a computational tradeoff—especially in cases where $q_{\max}$ is calculated using $\hat{M}$ and $\hat{M}$ is greater than M. When $\hat{M} \approx M$ and

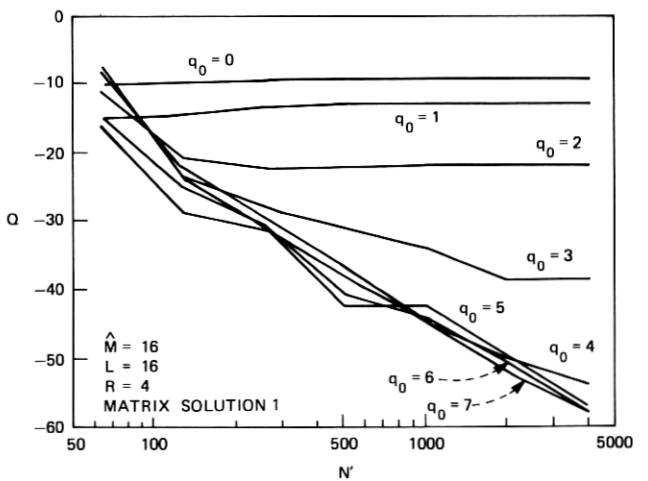

Fig. 4—Plots of Q versus N for $\hat{M} = 16$, $L = 16$, $R = 4$, s/n = ∞, and several values of q_0, using matrix solution method 1 [Section VI, step (*iv*)].

the impulse response of the system has large values near $n = \hat{M}$, then values of up to q_{max} are required for the best solutions.

Figure 5 shows plots of Q versus N for different Hamming window lengths L for the matrix solution method 1 (Fig. 5a) and for the FFT solution method 2 (Fig. 5b), for a fixed value of $\hat{M} = 8$ and for $\sigma_q^2 = 0$. (Comparable results were obtained for larger values of $\hat{M}$ up to $\hat{M} = 64$.) It can be seen by comparing the curves of Figs. 5a and 5b that the Q values obtained from the matrix solutions were from 10 to 20 dB better than those obtained from the FFT solution [Section VI, step (iv)] for small N (such that Q from the matrix solution was −30 dB or larger). For large N, the two methods of solution yielded essentially identical results.

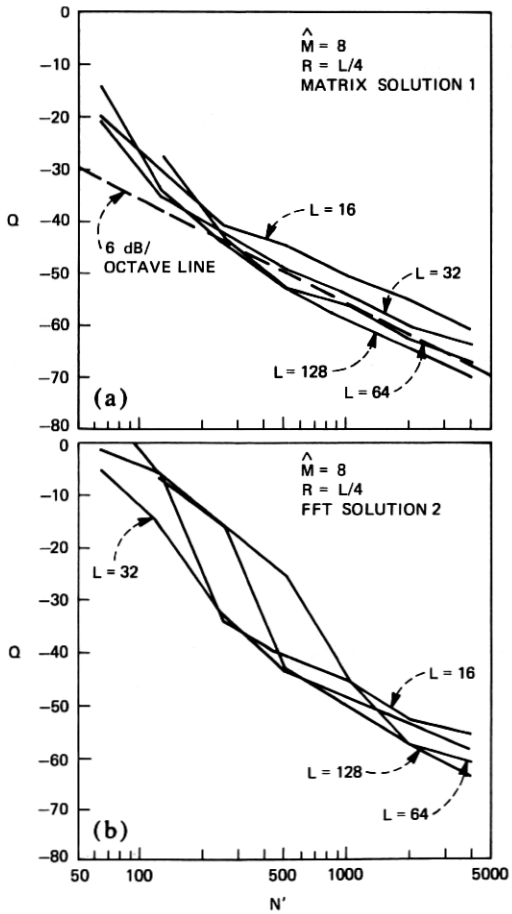

Fig. 5—Plots of Q versus N for $\hat{M} = 8$, $R = L/4$, s/n = ∞, and for several values of L for: (a) matrix method 1 and (b) FFT method 2 [Section VI, step (iv')].

From Figure 5a, two additional points are noted. First, we see that the asymptotic behavior of the curves of Q versus N is a 6-dB-per-octave slope as shown by the dotted line in this figure. For small N, the curves deviate from this slope. Second, we see small but consistent differences in the curve of Q versus N for different values of L. An exact explanation of this result is beyond the slope of this paper; however, eq. (39) shows that Q_Δ is directly proportional to the norm of $\boldsymbol{\delta} - \epsilon\hat{\mathbf{h}}$. It can be shown that $\|\boldsymbol{\delta} - \epsilon\hat{\mathbf{h}}\|$ gets smaller as L increases (since the error terms become more highly correlated), thus Q_Δ depends on L in a very complicated manner as illustrated in Fig. 5. A simple analysis of the effects of $\|\boldsymbol{\delta} - \epsilon\mathbf{h}\|$ on Q is as follows. If $\boldsymbol{\delta}$ and $\epsilon\mathbf{h}$ are not correlated, then

$$\|\boldsymbol{\delta} - \epsilon\mathbf{h}\| \approx \|\boldsymbol{\delta}\| + \|\epsilon\mathbf{h}\|. \tag{59}$$

When the two terms are correlated,

$$\|\boldsymbol{\delta} - \epsilon\mathbf{h}\| \ll \|\boldsymbol{\delta}\| + \|\epsilon\mathbf{h}\|. \tag{60}$$

Equation (59) implies that, if $\|\boldsymbol{\delta}\|$ is made zero, $\|\boldsymbol{\delta} - \epsilon\mathbf{h}\|$ decreases since one of two terms has been removed. Equation (60) implies that the error must greatly increase when $\|\boldsymbol{\delta}\| = 0$. Experimentally, $\boldsymbol{\delta}$ was set to 0 in our numerical simulations (by computing $\mathbf{r}$ exactly), and it was observed that the error Q increased by more than 20 dB. This showed that eq. (59) was a bad approximation because $\boldsymbol{\delta}$ and $\epsilon\mathbf{h}$ were highly correlated.

Figure 6 shows a direct comparison between the Q values obtained from the matrix solution method 1 (Section VI), the FFT solution method 2 (Section VI), and a third method which we call the classical Toeplitz case (solution method 3), for $\hat{M} = 8$ (Fig. 6a) and $\hat{M} = 64$ (Fig. 6b) and for $\sigma_q^2 = 0$. For the first two solution methods, a value of $L = 64$ was used for the window. Method 3, the classical Toeplitz case,[5] computes matrix elements $\hat{\phi}_T(l)$ and $\hat{\mathbf{r}}_T(l)$ directly from the data as

$$\hat{\phi}_T(l) = \sum_{n=\hat{M}-1}^{N-1-|l|} x(n)x(n+l)$$

$$\hat{r}_T(l) = \sum_{n=\hat{M}-1}^{N-1-|l|} x(n)y(n+l) \tag{61}$$

and determines $\hat{h}_T(n)$ as the solution of the matrix equation

$$\hat{\boldsymbol{\phi}}_T\hat{\mathbf{h}}_T = \hat{\mathbf{r}}_T. \tag{62}$$

By comparing the three solution methods, it is seen that the matrix solution method 1 gives the smallest Q values for almost the entire range of N, whereas the FFT method 2 gives smaller Q values than the

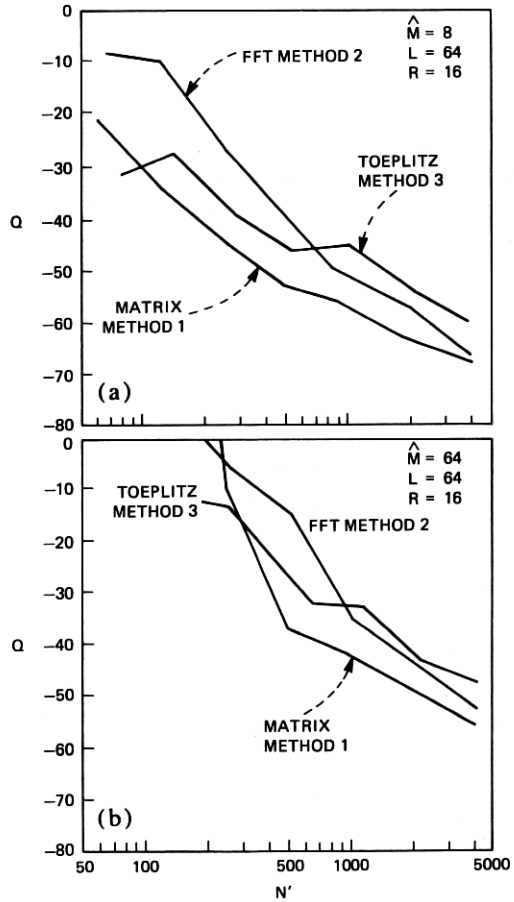

Fig. 6—Comparisons of the curves of Q versus N for $L = 64$, $R = 16$, s/n = ∞, for solution methods 1 to 3 for (a) $\hat{M} = 8$, and (b) $\hat{M} = 64$. Method 3 is defined in the text by eq. (62).

Toeplitz method 3 for large values of N, and larger Q values for small N. Analysis of the classical Toeplitz case shows that this method is identical to the matrix solution method 1 using a rectangular window with a shift of $R = L$ (i.e., an entire window shift). Figure 6 thus directly demonstrates that Hamming window results are better than rectangular window results.

Figure 7 shows a plot of Q versus $\hat{M}$ for a fixed value of $N = 1024$ and for several values of L. It can be seen that the curves of Q versus $\hat{M}$ have a slope of about 3 dB per octave in $\hat{M}$, as predicted based on the definition of eq. (5).[6] However, we also see the interesting effect that, for certain values of $\hat{M}$ and for different values of L, the value of Q makes a discrete jump and then jumps back to its previous level

(approximately). This effect is due to discrete changes in the limits q_1 and q_2 with L (see appendix) which is directly reflected in the curves of Q versus $\hat{M}$. The point of this figure is to show the effect of the positioning of the windows with respect to the data. Depending on the exact window placement, 3 dB of difference can be expected in a typical case.

As a final example, Fig. 8 shows a set of curves of Q vs N for s/n = 8 dB, $\hat{M} = 16$, and for several values of L. Also plotted in the figure is the theoretical curve[6] (dashed line) for the least-squares analysis $Q_{LSA} = 10 \log_{10}[\hat{M}/N] - \text{s/n}$. This curve drops at a rate of 3 dB per octave as N increases. It is seen that the measured Q curves from the matrix solution method 1 are quite close (within a few decibels) to the theoretical curve for values of N greater than about 100. In these cases, as N increases beyond about 100 points, the s/n-induced errors dominate the truncation (ϵ and δ induced) errors. Thus (for $N > 100$) there is no advantage in solving the LSA equation since the Toeplitz solution is equally accurate.

IX. DISCUSSION

The purpose of this paper has been to focus on the problems of system identification and spectral estimation and to investigate tech-

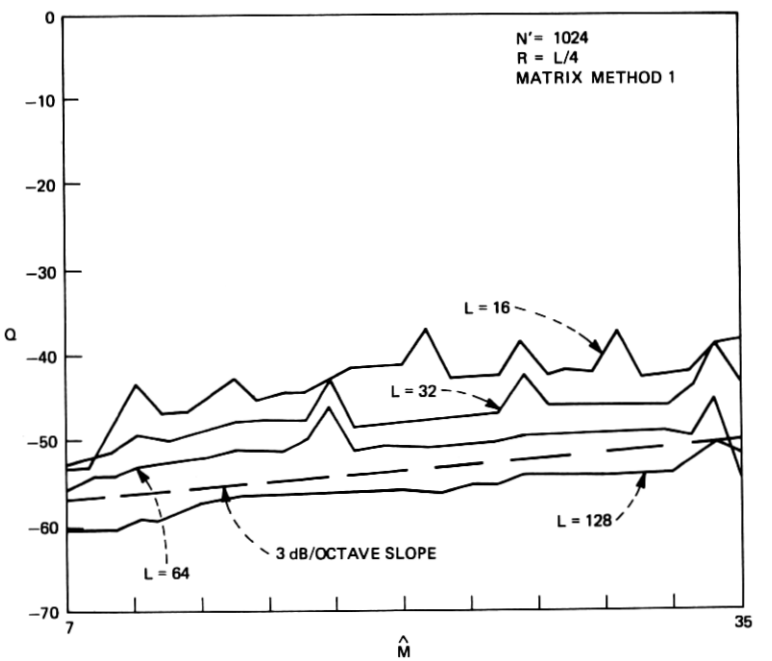

Fig. 7—Plots of Q versus $\hat{M}$ for $N = 1024$, $R = L/4$, s/n = ∞, and several values of L for matrix method 1. $\hat{M}$ is on a linear scale for this figure.

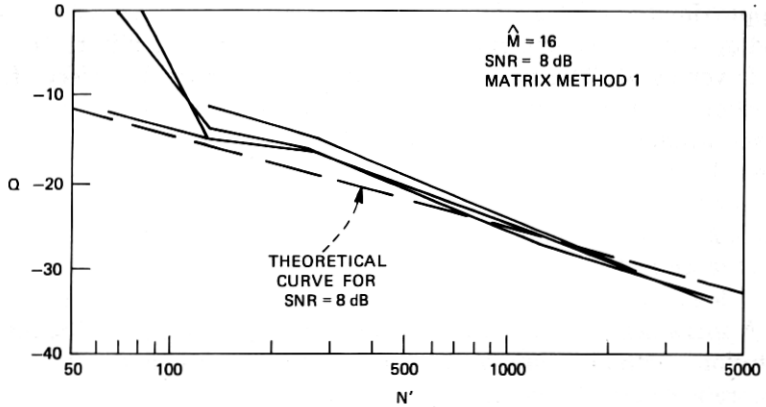

Fig. 8—Plots of Q versus N for $\hat{M} = 16$, s/n = 8 dB, and several values of L for matrix method 1. The dashed line is the theoretical LSA result for Q as derived in Ref. 6 (see text).

niques based on the short-time spectrum. We have shown that the problem of system identification can be solved by expanding each term of the least-squares solution in terms of short-time signals. By carefully examining and partitioning the terms entering into the computation, the system identification problem was approximately transformed from a general positive definite matrix inversion problem (the least-squares normal equations) to a Toeplitz matrix inversion problem with an error which was bounded and of order $1/N$. The terms which entered into the Toeplitz problem were identified as estimates of the power spectrum of the input and the cross power spectrum of the input and output. It was shown that the individual spectral estimates were unbiased—that is, they were independent of the window used to make the estimates.

Most of this paper has dealt with theoretical and numerical investigations of the properties of the resulting spectral estimates and their effect on the system identification solution. We have shown the following to be true:

(*i*) The spectral estimates $\mathbf{F}(\hat{\phi}(l))$ and $\mathbf{F}(\hat{r}(l))$ are unbiased.

(*ii*) The quality Q of the system identification estimate improves at a rate of 6 dB per octave as N increases for sufficiently large N and small additive noise (data-limited region).

(*iii*) The quality Q improves at a rate of 3 dB per octave as N increases for sufficiently large N and large additive noise (noise-limited region).

(*iv*) The resulting method approximates the least-squares normal equation by a Toeplitz equation, which is more accurate than the

standard Toeplitz approach which uses rectangular windows of duration equal to the total data length.

(*v*) The quality Q improves at a rate of 3 dB per octave as $\hat{M}$ decreases, if $\hat{M} \geq M$.

The key issue that remains to be discussed is the possible advantages and disadvantages of the short-time spectral approach [compared to alternative procedures such as the LSA or LMS (least-mean-squares[6] method)]. The main advantages of this method are:

(*i*) Implementation of the spectral estimates is straightforward and is readily performed using FFTs.

(*ii*) The resulting matrix equation can be solved directly using a Levinson[8] or Trench[9] inversion, or approximately via FFT methods.

(*iii*) The resulting solution has good asymptotic properties with respect to the variables N, $\hat{M}$, and s/n.

(*iv*) The method is easily amenable to adaptive procedures based on short-time spectral estimates. This property could be useful for systems where the additive noise is nonstationary—e.g., burst noise or corrupting speech.

(*v*) The method might potentially be applied to problems where $\hat{M}$ is on the order of 1000.

The disadvantages of the method are:

(*i*) The quality factor Q for the noiseless case for data lengths comparable to the impulse response duration ($N \approx M$) is significantly worse than that obtained from the LSA method.

(*ii*) A Toeplitz matrix equation must still be solved to obtain the highest accuracy solutions. However, it should be pointed out that the time required to invert a Toeplitz matrix is usually much less that the time required to compute it (i.e., when $N \gg \hat{M}$).

The final assessment of the utility of this, or any other spectral estimation or system identification method, is its applicability to a real world problem. One natural application for this method is the echo cancellation problem[10] where the impulse responses are long and possibly time-varying and additive nonstationary noise is present. We anticipate applying our technique to this problem as a more stringent test of its capabilities.

X. SUMMARY

In this paper, we have discussed a class of system identification and spectral estimation methods based on the short-time spectral representation of signals. We have discussed the properties of these methods and illustrated them with some simple examples. Our conclusion is that, for some applications, this new method provides a practical alternative to the classical least-squares analysis method. We would like to thank I. W. Sandberg for discussion on Section V.

APPENDIX

We derive here an explicit formula for $\hat{\phi}$ and ϵ. The constraints on N_A and N_B are

$$N_A \geq \hat{M} - 1 \tag{63}$$

$$N_B \leq N - 1 \tag{64}$$

$$N_A \leq N_B. \tag{65}$$

The equation for $\hat{\phi}(l - m)$ is

$$\hat{\phi}(l - m) = \sum_{q=q_1}^{q_2} \sum_{p=p_1}^{p_2} \phi_{p,p+q}(l, m), \tag{66}$$

where $\phi_{p,p+q}(l, m)$ is given by eq. (22) with $k = p + q$. Constraint (63) gives p_1, (64) gives p_2, and (65) gives q_1 and q_2 as follows. From eqs. (63) and (26),

$$pR \geq \hat{M} + L - 2 - \max(m, qR + l).$$

Since we wish this to hold for all lags (m, l) on $[0, \hat{M} - 1]$, it must hold for $m = l = 0$, the values which give the greatest p value for which the inequality holds. Thus

$$p_1(q) = \left\lceil \frac{\hat{M} + L - 2}{R} \right\rceil - \max(0, q). \tag{67}$$

The functions $\lceil x \rceil$ and $\lfloor x \rfloor$ are called CEILING(x) and FLOOR(x). They are defined by truncation to the next integer above and below x, respectively. For example, $\lceil \pi \rceil = 4$, $\lfloor -\pi \rfloor = -4$, $\lceil 0.5 \rceil = 1$, etc. For any x, $\lceil x \rceil = -\lfloor -x \rfloor$, $\lfloor x + n \rfloor = \lfloor x \rfloor + n$, and $\lceil x + n \rceil = \lceil x \rceil + n$, where n is an integer.

Constraint (64) gives p_2 with $m = l = \hat{M} - 1$ as the worst case. Using eq. (27),

$$p_2(q) = \left\lfloor \frac{N - \hat{M}}{R} \right\rfloor - \min(0, q). \tag{68}$$

Finally from constraint (65) and eqs. (26) and (27),

$$q_1 = \left\lceil \frac{m - l - L + 1}{R} \right\rceil \tag{69}$$

$$q_2 = \left\lfloor \frac{m - l + L - 1}{R} \right\rfloor. \tag{70}$$

Since p_1 and p_2 are functions of q, the $p(q)$ sum must be done first as shown in (66). Thus (66) to (70) completely specify $\hat{\phi}$.

Next we give formulas for ϵ. ϵ has two components, as may be seen in Fig. 3, which we call ϵ_+ and ϵ_-. Then $\epsilon = \epsilon_+ + \epsilon_-$, where

$$\epsilon_-(l, m) = \sum_{p=p_3}^{p_4} \sum_{k=k_3}^{k_4} \phi_{pk}(l, m) \tag{71}$$

with

$$p_3 = \left\lceil \frac{\hat{M} - 1 - m}{R} \right\rceil \tag{72}$$

$$k_4 = p_4 = \left\lfloor \frac{L + \hat{M} - 2}{R} \right\rfloor - 1 \tag{73}$$

$$k_3 = \left\lceil \frac{\hat{M} - 1 - l}{R} \right\rceil \tag{74}$$

and

$$\epsilon_+(l, m) = \sum_{p=p_5}^{p_6} \sum_{k=k_5}^{k_6} \phi_{pk}(l, m) \tag{75}$$

$$k_5 = p_5 = \left\lfloor \frac{N - \hat{M}}{R} \right\rfloor + 1 \tag{76}$$

$$p_6 = \left\lfloor \frac{N - 2 + L - m}{R} \right\rfloor \tag{77}$$

$$k_6 = \left\lfloor \frac{N - 2 + L - l}{R} \right\rfloor. \tag{78}$$

REFERENCES

1. L. R. Rabiner and Jont B. Allen, "Short-Time Fourier Analysis Techniques for FIR System Identification and Power Spectrum Estimation," IEEE Trans. Acoustics, Speech, and Signal Processing, *ASSP-27*, No. 2 (April 1979), pp. 182–192.
2. Jont B. Allen and R. Yarlagadda, "The Digital Poisson Summation Formula and One Application," unpublished work.
3. Jont B. Allen, "Short-Term Spectral Analysis, Synthesis, and Modification by Discrete Fourier Transform," IEEE Trans. Acoustics, Speech, and Signal Processing, *ASSP-25*, No. 3 (June 1977), pp. 235–238.
4. Jont B. Allen and L. R. Rabiner, "A Unified Approach to Short-Time Fourier Analysis and Synthesis," Proc. IEEE, *65*, No. 11 (November 1977), pp. 1558–1564.
5. G. M. Jenkins and D. G. Watts, *Spectral Analysis and Its Applications*, San Francisco: Holden-Day, 1968.
6. L. R. Rabiner, R. E. Crochiere, and Jont B. Allen, "FIR System Modelling and Identification in the Presence of Noise and Bandlimited Inputs," IEEE Trans. on Acoustics, Speech, and Signal Processing, *ASSP-26*, No. 4 (August 1978), pp. 319–333.
7. P. Eykhoff, *System Identification*, New York: John Wiley, 1974.
8. E. A. Robinson, "Multichannel Time Series Analysis with Digital Computer Programs," 2nd ed., San Francisco: Holden-Day, 1976, p. 44.
9. S. Zohar "Toeplitz Matrix Inversion: The Algorithm of W. F. Trench," J. Assoc. Comput. Mach. *16* (1967), pp. 592–601.
10. M. M. Sondhi, "An Adaptive Echo Cancellor," B.S.T.J., *46*, No. 3 (March 1967), pp. 497–511.
11. J. B. Allen, D. A. Berkley, and J. Blauert, "Multimicrophone Signal-Processing Technique to Remove Room Reverberation from Speech Signals," J. Acoust. Soc. Amer., *62*, No. 4 (October 1977), pp. 912–915.